Helicoidal magnetic ordering in double exchange systems

2005 J. Phys.: Condens. Matter 17 S753

(http://iopscience.iop.org/0953-8984/17/11/004)

INSTITUTE OF PHYSICS PUBLISHING JOURNAL OF PHYSICS: CONDENSED MATTER

J. Phys.: Condens. Matter **17** (2005) S753–S769 doi:10.1088/0953-8984/17/11/004

Helicoidal magnetic ordering in double exchange systems

Maxim Mostovoy

Max-Planck-Institut für Festkörperforschung, Heisenbergstrasse 1, D-70569 Stuttgart, Germany

Received 5 January 2005
Published 4 March 2005
Online at stacks.iop.org/JPhysCM/17/S753

Abstract

We show that double exchange does not always favour the ferromagnetic spin state. In transition metal oxides with strongly hybridized dp bands, the energy of conduction electrons can be minimized by an incommensurate helicoidal ordering of local spins. This explains the magnetic order observed in the iron perovskites $SrFeO_3$ and $CaFeO_3$. This homogeneous helicoidal state is stable against phase separation in a wide interval of electron concentrations.

(Some figures in this article are in colour only in the electronic version)

1. Introduction

The d electrons of transition metal ions can often be approximately divided into localized and itinerant ones. In metallic manganese and iron perovskites, $La_{1-x}Ca_xMnO_3$ and $SrFeO_3$, the charge is largely carried by the e_g electrons, while the t_{2g} electrons can be considered as spins localized on transition metal sites. A similar but less clear-cut distinction between the itinerant and localized t_{2g} electrons can be made in CrO_2 and LiV_2O_4 [1, 2]. On each transition metal site the strong Hund's rule coupling tends to align the spins of all the electrons. As a result, the kinetic energy of the conduction electrons strongly depends on the orientations of the local spins, forcing the latter to order in a way that minimizes the kinetic energy. This so-called double exchange mechanism [3–6] is responsible for strong correlations between transport and magnetism in the colossal magnetoresistance manganites [7].

Many properties of the double exchange systems can be described by the simple model [6]

$$H_{\rm DE} = -\sum_{ij\alpha\beta\sigma} t_{ij}^{\alpha\beta}\psi_{i\alpha\sigma}^{\dagger}\psi_{j\beta\sigma} - J\sum_{i\alpha\sigma\sigma'}\psi_{i\alpha\sigma'}^{\dagger}\frac{\boldsymbol{\sigma}_{\sigma'\sigma}}{2}\psi_{i\alpha\sigma}\cdot\mathbf{S}_i, \tag{1}$$

where the first term is the kinetic energy of conduction electrons, described by the operator $\psi_{i\alpha\beta}$ (i, α, σ are respectively the site, orbital and spin indices) and the second term is the Hund's rule coupling between the conduction electrons and local spins on the transition metal sites.

In the simplest approximation the local spins are treated classically and the coupling J is assumed to be infinitely strong. Then the spin of the conduction electron on the site i is parallel to the spin $\mathbf{S}_i$:

$$\psi_{i\alpha\sigma} = u_{i\sigma} c_{i\alpha},$$

where

$$u_i = \begin{pmatrix} \cos\frac{\theta_i}{2} \\ \sin\frac{\theta_i}{2} e^{i\phi_i} \end{pmatrix}$$

and θ_i, ϕ_i are the spherical angles describing the direction of $\mathbf{S}_i$. In this approximation equation (1) is equivalent to

$$H_{\mathrm{DE}} = -\sum_{ij} \tilde{t}_{ij}^{\alpha\beta} c_{i\alpha}^{\dagger} c_{j\beta}, \tag{2}$$

where the effective hopping amplitudes $\tilde{t}_{ij}^{\alpha\beta} = t_{ij}^{\alpha\beta} u_i^{\dagger} u_j$ for the polarized conduction electrons depend on the orientations of the local spins. Since $\tilde{t}_{ij}^{\alpha\beta} = t_{ij}^{\alpha\beta} \cos\frac{\theta_{ij}}{2}$, where $\theta_{ij} = \cos\theta_i \cos\theta_j + \sin\theta_i \sin\theta_j \cos(\phi_i - \phi_j)$ is the angle between the spins on the sites i and j, the hopping amplitudes are maximal for parallel spins. It seems, therefore, natural that the double exchange should favour ferromagnetic (FM) spin ordering, as in that case conduction bands are the widest.

In this paper we discuss non-collinear magnetic states in double exchange materials, and in particular, the helicoidal magnetic (HM) state in the iron perovskites $SrFeO_3$ and $CaFeO_3$. There are also reports about canted antiferromagnetic (AFM) states in doped manganites, e.g. $La_{1-x}Sr_xMnO_3$ for $0.06 < x < 0.09$ [12] and $Nd_{0.5}Sr_{0.5}MnO_3$ [13]. However, the interpretation of the coexisting FM and AFM spin correlations in terms of homogeneous canted states is often controversial due to the strong tendency of manganites towards the separation into FM and AFM phases [14].

Theoretical work on non-collinear magnetic states in double exchange systems was initiated by de Gennes [5], who considered the competition between the FM double exchange, described by equation (2), and the AFM superexchange:

$$H_{\mathrm{SE}} = J_A \sum_{\langle i,j \rangle} \mathbf{S}_i \cdot \mathbf{S}_j, \qquad J_A > 0. \tag{3}$$

When the kinetic energy of the conduction electrons is of the same order as the superexchange energy, the compromise can be a canted or a helicoidal state [5, 15, 16]. Since $J_A S^2$ is usually much smaller than the typical hopping amplitude t of the e_g electrons, the non-collinear ordering is expected to appear at low concentrations of charge carriers (electrons or holes), $n < \frac{2JS^2}{t}$ [5]. Precisely in this regime, however, homogeneous non-collinear states are unstable towards the FM–AFM phase separation, at least in simple free-electron models [14, 17–19]. It was argued that canted AFM states can also be stabilized in a wide range of electron concentrations by Fermi surface nesting, provided that the magnetic ordering occurs simultaneously with an orbital ordering [20].

The spin ordering, minimizing the energy of the model (1), is not always ferromagnetic. In particular, many rare earth materials, e.g. Ho and Er, which also can be described by this model (1), show a helicoidal ordering [21]. The on-site exchange interaction J of the localized f electrons of rare earth ions with conduction electrons is weak compared to the conduction band width. Treated perturbatively, it gives rise to the oscillating long-range RKKY interaction between the f-electron moments [22],

$$H_{\mathrm{RKKY}} = \tfrac{1}{2} \sum_{i,j} J_{ij} \mathbf{S}_i \cdot \mathbf{S}_j, \tag{4}$$

which, in general, favours an incommensurate non-collinear magnetic ordering. The ferromagnetic state can also become unstable for large fillings of the majority band [23, 24].

In this paper we show that even in the infinite J limit the double exchange mechanism alone can favour helicoidal magnetic ordering. We argue that the helicoidal ordering observed in the iron perovskites $SrFeO_3$ and $CaFeO_3$ is a direct consequence of an anomalously large negative charge transfer energy in these materials.

The rest of the paper is organized as follows. Section 2 contains a general discussion of the instability of the FM state in double exchange systems towards helicoidal spin ordering. In section 3 we briefly review the magnetic and transport properties of iron perovskites and formulate a simple model that describes double exchange in dp metals. The magnetic ground states of this model are discussed in section 4, where we also give a simple estimate of the critical value of the charge transfer energy, at which the FM state becomes unstable. In section 5 we study the stability of homogeneous helicoidal states against separation and in section 6 we calculate the spectrum of magnetic excitations and close to the transition between the ferromagnetic and helicoidal states. Finally, we conclude in section 7. For completeness we use here some of our results previously reported in [25].

2. Instability of ferromagnetic state towards helicoidal ordering

It may seem somewhat counterintuitive that the kinetic energy of conduction electrons can reach a minimum for a non-collinear ordering of local spins. In this section we clarify the mechanism of the instability of the FM state in double exchange systems.

Consider the helicoidal state with the wavevector $\mathbf{Q}$ and spin rotation axis $\hat{\mathbf{x}}$:

$$\boldsymbol{\sigma}\cdot\mathbf{S}_j = S\left(\sigma_z\cos\mathbf{Q}\cdot\mathbf{x}_j + \sigma_y\sin\mathbf{Q}\cdot\mathbf{x}_j\right) = \mathrm{e}^{\frac{\mathrm{i}}{2}\sigma_x\mathbf{Q}\cdot\mathbf{x}_j}\sigma_z\mathrm{e}^{-\frac{\mathrm{i}}{2}\sigma_x\mathbf{Q}\cdot\mathbf{x}_j}, \tag{5}$$

where the vector $\mathbf{x}_j$ describes the position of the site j. Performing the transformation to the spin frame with the z axis on the site j parallel to $\mathbf{S}_j$,

$$\psi_{j\alpha} = \mathrm{e}^{\frac{\mathrm{i}}{2}\sigma_x\mathbf{Q}\cdot\mathbf{x}_j}\psi'_{j\alpha}, \tag{6}$$

we can write the interaction between the localized and itinerant electrons (the second term in equation (1)) in the form it has for the FM state:

$$-\frac{JS}{2}\sum_{j\alpha}{\psi'_{j\alpha}}^{\dagger}\sigma_z\psi'_{j\alpha}. \tag{7}$$

The transformation (6), however, modifies the form of the kinetic energy operator T (the first term in equation (1)). Combining the Fourier transformation with the spin rotation,

$$\psi_{j\alpha} = \frac{1}{\sqrt{N}}\sum_{\mathbf{k}}\mathrm{e}^{\mathrm{i}\left(\mathbf{k}+\frac{\sigma_x}{2}\mathbf{Q}\right)\cdot\mathbf{x}_j}c_{\mathbf{k}\alpha}, \tag{8}$$

where N is the number of transition metal sites, we obtain

$$T = \sum_{\mathbf{k}\alpha}c^{\dagger}_{\mathbf{k}\alpha}t^{\alpha\beta}_{\mathbf{k}+\frac{\sigma_x}{2}\mathbf{Q}}c_{\mathbf{k}\beta}, \tag{9}$$

where

$$t^{\alpha\beta}_{\mathbf{k}+\frac{\sigma_x}{2}\mathbf{Q}} = \sum_j\mathrm{e}^{-\mathrm{i}\left(\mathbf{k}+\frac{\sigma_x}{2}\mathbf{Q}\right)\cdot\left(\mathbf{x}_j-\mathbf{x}_0\right)}t^{\alpha\beta}_{j0}. \tag{10}$$

For small $\mathbf{Q}$, we have

$$\begin{aligned} T &\approx T^{(0)} + T^{(1)} + T^{(2)} \\ &= \sum_{\mathbf{k}\alpha}\left[c^{\dagger}_{\mathbf{k}\alpha}t^{\alpha\beta}_{\mathbf{k}}c_{\mathbf{k}\beta} + c^{\dagger}_{\mathbf{k}\alpha}\sigma_x\partial t^{\alpha\beta}_{\mathbf{k}}c_{\mathbf{k}\beta} + \tfrac{1}{2}c^{\dagger}_{\mathbf{k}\alpha}\partial^2 t^{\alpha\beta}_{\mathbf{k}}c_{\mathbf{k}\beta}\right], \end{aligned} \tag{11}$$

where $\partial = \frac{1}{2}\mathbf{Q}\cdot\nabla_{\mathbf{k}}$. To the second order in Q the difference between energies of the HM and FM states is

$$\delta E^{(2)} = -\sum_{\nu}\frac{\left|\langle\nu|T^{(1)}|0\rangle\right|^2}{E_\nu - E_0} + \langle 0|T^{(2)}|0\rangle. \tag{12}$$

In the first term ν labels the spin-flip excitations, since the operator $T^{(1)}$ flips one spin. This negative term is the energy gain due to the mixing of spin-up and spin-down electron states for helicoidally ordered spins, which lowers the energies of the occupied states. The second term in equation (12) describes the energy loss due to the band narrowing caused by the rotation of the local spins. It is positive and favours FM ordering. When the chemical potential in the FM state is close to the bottom of the empty spin-down band, the spin-flip excitation energy $E_\nu - E_0$ can be low and the gain due to the transition to the helicoidal state can exceed the loss. A simple solvable model showing such a transition is discussed in the appendix.

In the double exchange model (1), used to describe doped manganites, conduction electrons can only reside on transition metal sites occupied by local spins. In that case, the strong Hund's rule coupling J results in a large exchange splitting of the spin-up and spin-down bands and the FM state can only be unstable for large fillings of the conduction bands. Furthermore, one can show that for the quadratic dispersion of the conduction electrons the instability may not occur even when the chemical potential exceeds the lowest energy of the spin-down band, i.e. the unsaturated magnetic state has a lower energy than the helicoidal one (see the appendix).

A different situation occurs in transition metal oxides with strongly covalent conduction bands. In these materials charge carriers with a high probability occupy oxygen sites, on which there are no local spins. In section 4 we show that in this case the density of low energy spin-flip excitations can be sufficiently high to stabilize the HM ordering.

3. Double exchange in dp metals

In the perovskites $SrFeO_3$, $CaFeO_3$, Sr_2FeO_4 and $Sr_3Fe_2O_7$, iron is in a rather high oxidation state, Fe^{4+}. Although Fe^{4+} nominally has the same d^4 configuration as the Mn^{3+} ion in $LaMnO_3$, the structural, magnetic and transport properties of ferrates are different from those of manganites.

While in $LaMnO_3$ the Jahn–Teller effect plays an important role [7, 26], no orbital ordering has been observed in ferrates. In the case of $SrFeO_3$, which remains metallic and perfectly cubic down to 4 K [27], the suppression of orbital ordering can be ascribed to wide conduction bands: the Fe–O–Fe angle in $SrFeO_3$ is 180°. However, the ferrates with more localized electrons, e.g. $CaFeO_3$, in which the Fe–O–Fe angle is close to the Mn–O–Mn angle in $LaMnO_3$, also show no Jahn–Teller instability. Instead, they undergo a metal–insulator transition to a charge-ordered state. At $T_{CO} = 290$ K, $CaFeO_3$ shows the $BaBiO_3$-type of charge ordering, i.e. the charge disproportionation $2Fe^{4+} \rightarrow Fe^{(4+\delta)+} + Fe^{(4-\delta)+}$ with the concomitant alternation of larger and smaller oxygen octahedra [10, 11, 28, 29]. A similar charge ordering has been observed in $Sr_3Fe_2O_7$ at $T_{CO} = 343$ K [30–32].

The types of magnetic ordering found in iron and manganese perovskites are also very different. In manganites, magnetism is strongly coupled to transport: insulators, such as $LaMnO_3$ and $CaMnO_3$, exhibit commensurate AFM orderings, while metals, e.g. $La_{1-x}Sr_xMnO_3$ for $0.2 < x < 0.5$, are ferromagnetic. Furthermore, in a wide range of doping, manganites show the separation on FM and AFM phases [14]. In contrast, metallic $SrFeO_3$ and insulating $CaFeO_3$ show an incommensurate HM ordering with close values of the helix wavevector $\mathbf{Q}$ and Néel temperature: $\frac{\mathbf{Q}}{2\pi} = 0.11(1, 1, 1)$, $T_N = 134$ K for $SrFeO_3$ [8, 9]

and $\frac{\mathbf{Q}}{2\pi} = 0.16(1, 1, 1)$, $T_N = 115$ K for $CaFeO_3$ [10, 11]. The helicoidal ordering in ferrates seems to be robust and independent of transport. In particular, no resistivity anomaly at the Néel temperature has been observed in $SrFeO_3$, in sharp contrast to the colossal magnetoresistance effect observed in manganites [33].

The suppression of orbital ordering in ferrates was related to an anomalously low charge transfer energy (i.e. the energy necessary to transfer an electron from an oxygen to a transition metal ion), $\Delta \approx -3$ eV, found in photoemission experiments on $SrFeO_3$ and $CaFeO_3$ [34, 35]. For large negative Δ, the conduction bands are formed by the strongly hybridized iron e_g and oxygen p_σ orbitals [36]. A high density of oxygen holes implies high probability for Fe ions to be in the non-degenerate d^5 electronic configuration, which suppresses the Jahn–Teller instability. On the other hand, the Coulomb energy cost of the charge ordering is greatly reduced when the ordering occurs on the O–O and O–Fe bonds rather than on the Fe sites. The suppression of orbital ordering by the intervening charge ordering was also observed in rare earth nickelates—another class of Jahn–Teller materials with low Δ [37, 38].

In the remainder of this section we formulate a simple model, which describes double exchange in dp metals [25]. In this model the degree of the hybridization of the transition metal and oxygen bands can be tuned, and in the limit of large positive charge transfer energy Δ this model becomes equivalent to the double exchange model (2). We assume that on each transition metal site three t_{2g} electrons form a net spin $3/2$. Furthermore, the Hund's rule coupling is assumed to be infinitely strong, so that the spins of the e_g electrons are parallel to the local spins. In addition, we explicitly consider the states with holes on the oxygen p_σ orbitals that are strongly hybridized with the transition metal e_g orbitals.

It is convenient to describe the states of dp metals in terms of holes, which can occupy oxygen and transition metal sites. By holes on transition metal sites we mean the e_g holes in the high-spin electronic d^5 configuration with the total spin $S = 5/2$. For infinite Hund's rule coupling the spin of the e_g hole on the site i is antiparallel to the local spin $\mathbf{S}_i = S(\sin\theta_i \sin\phi_i, \cos\theta_i \sin\phi_i, \cos\theta_i)$. The spin state of such a hole is described by the spinor

$$v_i = \begin{pmatrix} -\sin\frac{\theta_i}{2} e^{-i\phi_i} \\ \cos\frac{\theta_i}{2} \end{pmatrix}, \tag{13}$$

while other degrees of freedom are described by the operator $d_{i\alpha}$, where the index $\alpha = 3z^2 - r^2, x^2 - y^2$ labels the e_g orbital.

The model Hamiltonian describing the double exchange in dp metals has the form

$$H_{dp} = \sum_{i\alpha b} t_{\alpha b} \left(d^\dagger_{i\alpha} v^\dagger_i P_{ib} + P^\dagger_{ib} v_i d_{i\alpha} \right) + t_{pp} \sum_{i, b\neq c} P^\dagger_{ib} P_{ic} + \Delta \sum_{ib} p^\dagger_{i+b/2} p_{i+b/2}, \tag{14}$$

where

$$p_{i\pm b/2} = \begin{pmatrix} p_{i\pm b/2\uparrow} \\ p_{i\pm b/2\downarrow} \end{pmatrix}, \qquad b = x, y, z,$$

annihilates the hole on one of the six oxygen ions from the octahedron with the centre at the transition metal site i and $P_{ib} = p_{i+b/2} + p_{i-b/2}$. In equation (14) the operator P_{ib} is projected on the spinor v_i, since the hopping on the site i is only allowed for holes with the spin antiparallel to the iron spin $\mathbf{S}_i$. With the exception of section 6, in which we discuss magnetic excitations, the local spins are assumed to be classical.

The amplitudes of hopping between the e_g and p_σ orbitals are given by

$$t_{3z^2-r^2,b} = (pd\sigma)(-\tfrac{1}{2}, -\tfrac{1}{2}, 1), \qquad t_{x^2-y^2,b} = (pd\sigma)\left(\frac{\sqrt{3}}{2}, -\frac{\sqrt{3}}{2}, 0\right),$$

and $t_{pp} = \frac{1}{2}(pp\sigma) - \frac{1}{2}(pp\pi)$ is the hopping amplitude between two neighbouring oxygen sites. Here $(pd\sigma)$, $(pp\sigma)$ and $(pp\pi)$ are the Slater–Koster parameters [39], which for holes have the sign opposite to that for electrons.

In this paper we do not take into account the Coulomb repulsion between holes on transition metal sites, since for large negative Δ the probability for two holes to occupy the same iron ion (the d^3 state with empty e_g levels) is already rather small. We assume, however, that long range Coulomb interactions suppress large fluctuations of the hole density and perform all calculations for the fixed density $n = 1$ (1 hole/Fe) rather than fixed chemical potential.

In the limit of large positive charge transfer energy, $\Delta \to +\infty$, the low-energy sector of the dp model (14) is equivalent to the double exchange dd model (2), in which holes only occupy transition metal sites and the spin ordering is ferromagnetic. In the next section we show that the dp model can have an incommensurate helicoidal or even the A-type antiferromagnetic ground state, even though the Hamiltonian (14) does not include the superexchange interaction between local spins (3).

4. Helicoidal magnetic ordering

Consider the helicoidal state with the wavevector $\mathbf{Q}$ and spin rotation axis $\mathbf{e}$. Due to the invariance of the Hamiltonian (14) under an arbitrary rotation of all spins, the energy of the helicoidal state is independent of direction of the spin rotation axis $\mathbf{e}$. For $\mathbf{e} = \hat{x}$, the spin of the transition metal ion j is given by

$$\mathbf{S}_j = S\left(\hat{z}\cos\mathbf{Q}\cdot\mathbf{x}_j + \hat{y}\sin\mathbf{Q}\cdot\mathbf{x}_j\right), \tag{15}$$

so that the spinor v_j describing the polarization of the hole on this site (see equation (13)) is

$$v_j = \mathrm{e}^{\frac{\mathrm{i}}{2}\sigma_x(\mathbf{Q}\mathbf{x}_j)}\begin{pmatrix}0\\1\end{pmatrix}.$$

To find the hole dispersion for this helicoidal state, we combine the Fourier transformation with the spin rotation that aligns the z axis on the site j with the local spin $\mathbf{S}_j$:

$$\begin{aligned} d_{\mathbf{k}\alpha} &= \frac{1}{\sqrt{N}}\sum_j \mathrm{e}^{-\mathrm{i}\mathbf{k}\mathbf{x}_j} d_{j\alpha},\\ p_{\mathbf{k}b} &= \frac{1}{\sqrt{N}}\sum_j \mathrm{e}^{-\mathrm{i}\left(\mathbf{k}+\frac{1}{2}\sigma_x\mathbf{Q}\right)\mathbf{x}_{j+b/2}} p_{j+b/2},\\ P_{\mathbf{k}b\sigma} &= 2\cos\frac{Q_b}{4}\cos\frac{k_b}{2}p_{\mathbf{k}b\sigma} - 2\sin\frac{Q_b}{4}\sin\frac{k_b}{2}p_{\mathbf{k}b,-\sigma}, \end{aligned} \tag{16}$$

where N is the number of Fe sites. The Hamiltonian (14) then reads

$$H_{dp} = \sum_{\mathbf{k}\alpha b} t_{\alpha b}\left(d^\dagger_{\mathbf{k}\alpha}P_{\mathbf{k}b\downarrow} + P_{\mathbf{k}b\downarrow}{}^\dagger d_{\mathbf{k}\alpha}\right) + t_{pp}\sum_{\mathbf{k},b\neq c} P_{\mathbf{k}b}{}^\dagger P_{\mathbf{k}c} + \Delta\sum_{\mathbf{k}b} p_{\mathbf{k}b}{}^\dagger p_{\mathbf{k}b}. \tag{17}$$

Consider first the FM state with $\mathbf{S}_j = S\hat{z}$. In figure 1 we plot the spin-down bands (solid curves) and spin-up bands (circles), calculated for $(pd\sigma) = 1.7$ eV, $t_{pp} = 0.65$ eV and $\Delta = -2$ eV, which is a typical set of parameters for iron perovskites [34, 35, 40]. In the Fermi sea holes occupy the two lowest spin-down bands formed by the hybridized $d_\downarrow$ and $p_\downarrow$ states (the chemical potential μ for $n = 1$ is shown by the thin horizontal line). The spin-up bands are formed by $p_\uparrow$ holes, since in the FM state the hopping of the spin-up holes on transition metal sites is forbidden. The energy of these purely oxygen states is higher than those of the occupied $dp_\downarrow$ states. However, for the large negative $\Delta = -2$ eV, the energy separation between the unoccupied spin-up and occupied spin-down states is sufficiently small to make this FM state

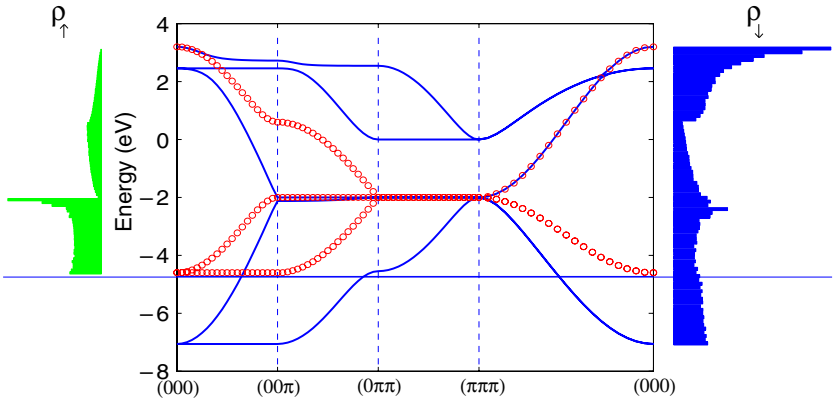

Figure 1. The hybridized $dp_{\downarrow}$-hole bands (solid curves) and oxygen p↑-hole bands (circles) for ferromagnetically ordered local spins, $(pd\sigma) = 1.7$ eV, $t_{pp} = 0.65$ eV and $\Delta = -2$ eV. Plotted from the left (right) is the corresponding density of the spin-up (spin-down) states. The thin horizontal line indicates the Fermi level for 1 e_g hole per Fe.

unstable. For a helix with the wavevector along the body diagonal, $\mathbf{Q} = \phi(1, 1, 1)$, the optimal value of the angle ϕ between spins in neighbouring [111] layers is 0.937.

As was discussed in section 1, this instability is driven by the energy gained due to the mixing of the occupied and unoccupied states with opposite spin projections (for $Q \neq 0$, $P_{\mathbf{k}b\downarrow}$ in equation (17) is the sum of the spin-down and spin-up oxygen hole operators $p_{\mathbf{k}b\sigma}$, reflecting the fact that in the helicoidal state spin is not conserved). Figure 2 shows the effect of the FM–HM transition on the total density of the hole states. Near the bottom of the Fermi sea the density of states decreases due to the band narrowing in the helicoidal state, which results in an energy loss. This loss, however, is overcompensated by the energy gain due to the mixing of the spin-up and spin-down hole states for $Q \neq 0$, which lowers the energies of the occupied levels and results in an increase of the density of states in the rest of the Fermi sea.

An estimate of the critical charge transfer energy Δ_c, at which the FM ground state becomes unstable, can be obtained as follows. From equation (17) we find that the minimal and maximal energies for the two lowest $dp_{\downarrow}$ bands are

$$\varepsilon_{\downarrow}(\mathbf{k} = (0, 0, 0)) = \frac{\Delta - 4t_{pp}}{2} - \sqrt{\left(\frac{\Delta - 4t_{pp}}{2}\right)^2 + 6(pd\sigma)^2},$$
$$\varepsilon_{\downarrow}(\mathbf{k} = (\pi, \pi, \pi)) = \Delta. \tag{18}$$

Figure 1 shows that the density of states in these two half-filled bands is roughly independent of energy. Then the chemical potential is approximately given by

$$\mu \sim \tfrac{1}{2}\left[\varepsilon_{\downarrow}(0, 0, 0) + \varepsilon_{\downarrow}(\pi, \pi, \pi)\right]. \tag{19}$$

The bottom of the purely oxygen $p_{\uparrow}$ band lies at

$$\varepsilon_{\uparrow}(0, 0, 0) = \Delta - 4t_{pp}. \tag{20}$$

Assuming that the FM–HM transition occurs at $\mu \sim \varepsilon_{\uparrow}(0, 0, 0)$, we obtain a simple expression:

$$\Delta_c \sim -\frac{\left(3(pd\sigma)^2 - 16t_{pp}^2\right)}{2t_{pp}}. \tag{21}$$

For instance, for $(pd\sigma) = 1.3$ eV and $t_{pp} = 0.4$ eV, equation (21) gives $\Delta_c \sim -3$ eV (from numerical calculations we obtain $\Delta_c = -2.75$ eV (see figure 3)), which is close to

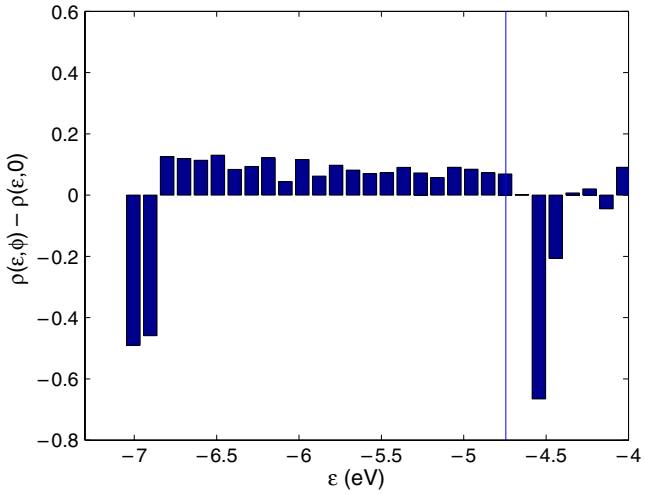

Figure 2. The difference between the densities of hole states for HM and FM orderings, calculated for $(\mathrm{pd}\sigma) = 1.7$ eV, $t_{\mathrm{pp}} = 0.65$ eV, $\Delta = -2$ eV and the optimal angle for the HM state $\phi = 0.937$. The vertical line indicates the position of the Fermi energy for the FM state.

$\Delta = -3.1$ eV, found for $SrFeO_3$ in the photoemission experiment [34]. This shows that the HM ordering in ferrates largely results from the double exchange.

The instability of the FM state towards HM ordering is similar to the spin-density-wave instability. However, while the latter requires a nested Fermi surface and results in a gap opening, the transition from the FM to the HM state is not very sensitive to the shape of the Fermi surface and, in general, does not open a gap. Figure 2 shows that the energy gain is distributed over the whole Fermi sea and shows no peak at the Fermi energy, as would be the case for the spin-density-wave state. The crossing of the spin-up and spin-down bands at the Fermi surface of the FM state only occurs at isolated points, so that the mixing of these bands in the helicoidal state does not open a gap in the density of states. Thus the FM–HM instability is a Fermi sea rather than a Fermi surface instability and, therefore, it can also occur in insulators with a small gap, e.g. $CaFeO_3$ [25]. This explains the apparent decoupling of transport and magnetism in ferrates.

The effects of pressure on magnetic ordering in $SrFeO_3$ and $CaFeO_3$ were studied in Mössbauer spectroscopy experiments [41, 42], which showed that the magnetic transition temperature grows with increasing pressure. At high pressures (7 GPa for $SrFeO_3$) the spin ordering becomes ferromagnetic. The growth of the transition temperature can be readily explained by an increase of the band width upon applied pressure, which makes the double exchange between the local spins stronger. Furthermore, for wider conduction bands the ratio $\frac{|\Delta|}{(\mathrm{pd}\sigma)}$ becomes smaller. The dependence of the helical angle ϕ, for $\mathbf{Q} = \phi(1, 0, 0)$, $(\mathrm{pd}\sigma) = 1.3$ eV and $t_{\mathrm{pp}} = 0.4$ eV, is shown in figure 3. The pitch of the helix monotonically decreases with decreasing $|\Delta|$, until the spin ordering becomes ferromagnetic ($\phi = 0$).

Figure 4 shows the dependence of the energy of the double exchange model (1) on the direction of the wavevector $\mathbf{Q}$ (squares). The minimum of energy is reached for $\mathbf{Q}$ parallel to one of the cubic axes, e.g. $Q \parallel [100]$. Thus, close to the transition between HM and FM states, the Landau expansion of the double exchange energy is

$$E_{\mathrm{DE}}(\mathbf{Q}) - E_{\mathrm{DE}}(0) = aQ^2 + \frac{b}{2}Q^4 - \frac{c}{2}\left(Q_x^4 + Q_y^4 + Q_z^4\right), \tag{22}$$

with $b > c > 0$.

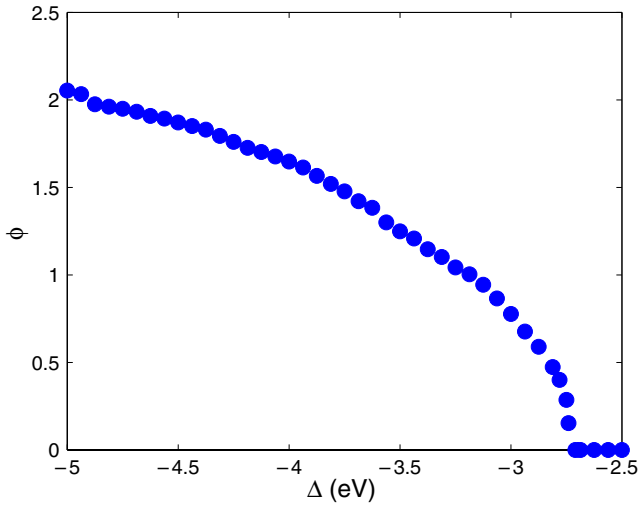

Figure 3. The angle ϕ between the spins in neighbouring [100] layers ($\mathbf{Q} = \phi(1, 0, 0)$) plotted versus Δ for $(\mathrm{pd}\sigma) = 1.3$ eV and $t_{\mathrm{pp}} = 0.4$ eV.

On the other hand, in iron helimagnets the wavevector is pointing along the body diagonal, e.g. in $SrFeO_3$, $\mathbf{Q} \approx 0.7(1, 1, 1)$ [8]. Note, however, that close to the FM–HM transition, when the helix wavevector is small, the dependence of the double exchange energy on the direction of $\mathbf{Q}$ is extremely weak. (In figure 4 the energy is counted from its value at $\hat{Q} = (1, 0, 0)$, which for the double exchange model is ~ -6.5 eV/Fe.) Therefore, the direction of the helix wavevector can be affected by relatively weak interactions, and in particular, the AFM superexchange (3). For small Q the superexchange energy per spin is given by

$$E_{\mathrm{SE}}(\mathbf{Q}) - E_{\mathrm{SE}}(0) = J_A S^2 \left[-\tfrac{1}{2} Q^2 + \tfrac{1}{24} \left(Q_x^4 + Q_y^4 + Q_z^4 \right) \right]. \tag{23}$$

Thus, the sum of the double exchange and superexchange energy has a minimum for $\mathbf{Q}$ along the body diagonal for $J_A S^2 > 12c$. In figure 4 we show the dependence of $E_{\mathrm{DE}} + E_{\mathrm{SE}}$ on the direction of $\mathbf{Q}$ for $J_A S^2/(\mathrm{pd}\sigma) = 0.024$ (circles), which has a minimum for $\mathbf{Q} \parallel (1, 1, 1)$. The value of $JS^2/(\mathrm{pd}\sigma)$ necessary to change the orientation of the helix is small, because the double exchange system itself is magnetically soft close to the transition between FM and HM states. Thus, although the AFM superexchange may affect the wavevector $\mathbf{Q}$, it is not the main reason for the HM ordering in ferrates.

It is instructive to consider the limit $-\Delta \gg (\mathrm{pd}\sigma)$, in which holes reside mainly on oxygen ions, while the iron ions are in the d^5 state with $S = \frac{5}{2}$. The coupling between the holes and spins $\propto \frac{(\mathrm{pd}\sigma)^2}{\Delta}$ can then be treated perturbatively and the double exchange reduces to the effective RKKY interaction (4) between the iron spins, mediated by the particle–hole excitations propagating over the oxygen sites. The energy of the helicoidal ground state (15) is proportional to the Fourier transform of the RKKY coupling

$$J_{\mathbf{Q}} = \sum_j \mathrm{e}^{-\mathrm{i}\mathbf{Q}\cdot(\mathbf{x}_j - \mathbf{x}_0)} J_{j0}$$

and $J_{\mathbf{Q}}$ has a minimum at the optimal helix wavevector $\mathbf{Q}$. The plot of $-J_{\mathbf{Q}}$ along a path in the Brillouin zone (see figure 5) shows that this RKKY interaction favours $\mathbf{Q} = \pi(1, 0, 0)$, corresponding to the A-type antiferromagnetic state. Thus, the helicoidal magnetic ordering with $\mathbf{Q} = Q(1, 0, 0)$ interpolates between the ferromagnetic ordering at large positive Δ and the A-type antiferromagnetic ordering at large negative Δ.

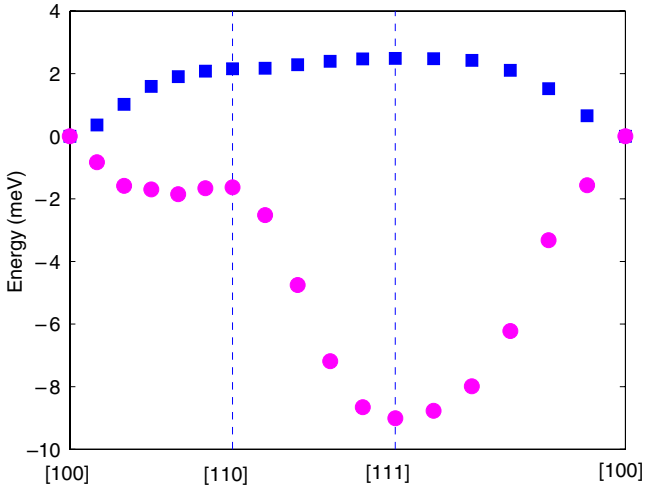

Figure 4. The energy/Fe as a function of the direction of the helix wavevector $\hat{Q}$ for the double exchange model (squares) and for the double exchange + superexchange model with $J_A S^2/(\mathrm{pd}\sigma) = 0.024$ (circles). The energy is counted from its value at $\hat{Q} = (1, 0, 0)$. Other parameters used in this calculation are $(\mathrm{pd}\sigma) = 1.7$ eV, $t_{\mathrm{pp}} = 0.6$ eV and $\Delta = -3$ eV.

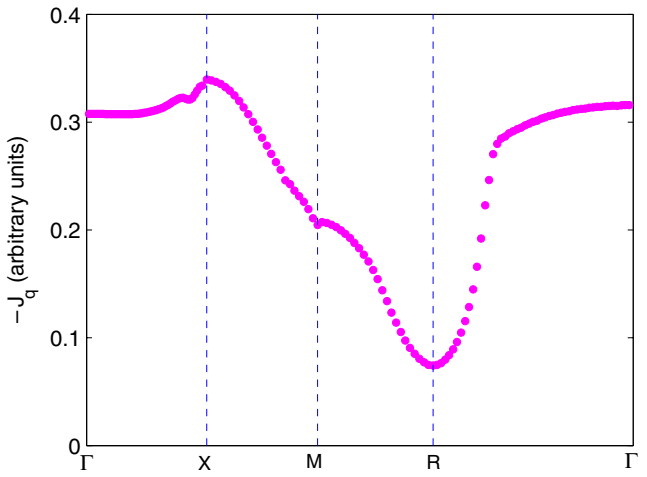

Figure 5. The **Q** dependence of the Fourier transform $-J_{\mathbf{Q}}$ of the RKKY interaction in the limit of large negative Δ.

5. Electronic compressibility

It was noted long ago that the homogeneous canted/helicoidal de Gennes state, resulting from the competition between the FM double exchange and AFM superexchange, is unstable towards the separation into the FM phase containing all charge carriers and the insulating AFM phase [17]. This can be seen from the fact that the electronic compressibility κ of this state, defined by

$$\kappa^{-1} = \frac{\mathrm{d}\mu}{\mathrm{d}n}, \tag{24}$$

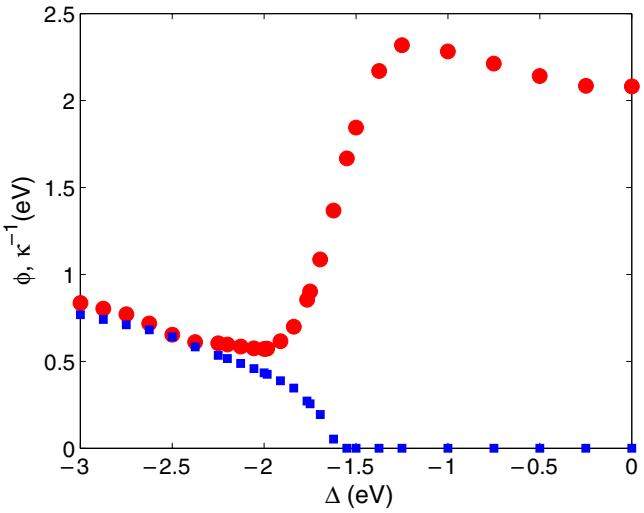

Figure 6. The dependence of the helical angle ϕ (squares) and inverse compressibility κ^{-1} (circles) versus Δ for $(\mathrm{pd}\sigma) = 1.7$ eV, $t_{\mathrm{pp}} = 0.65$ eV, and $n = 1$.

where n is the charge carrier density, is negative [18, 19]. The chemical potential μ decreases with increasing n due to the fast growth of the conduction band width in the de Gennes non-collinear state.

In principle, the negative electronic compressibility obtained within the free-electron model (2) does not necessarily imply the instability towards phase separation, as the latter can be suppressed by Coulomb interactions. But the phase separation is, in fact, ubiquitous in manganites [14]. It is, therefore, of interest to study the stability towards phase separation of the helicoidal state favoured by the double exchange for large negative Δ.

Figure 6 shows the dependence of κ^{-1} on Δ close to the FM–HM transition. The jump of the compressibility at the transition point generally follows from the Landau expansion of energy in powers of the helical wavevector Q. Although the electronic compressibility of the HM state for $\Delta \sim -2$ eV is much higher than that of the FM state, it remains positive, i.e. the helicoidal state is stable against phase separation.

In figure 7(a) we plot the dependence of the helical angle ϕ on the density of holes n for $(\mathrm{pd}\sigma) = 1.7$ eV, $t_{\mathrm{pp}} = 0.65$ eV and $\Delta = -2$ eV. For these parameters the (second-order) transition from the FM to the HM state occurs at n slightly less than 1. The angle ϕ grows with increasing hole density. This growth is terminated by the first-order transition to the A-type AFM state.

Figure 7(b) shows the corresponding density dependence of the hole chemical potential μ. Close to the transition to the AFM state $\frac{\mathrm{d}\mu}{\mathrm{d}n}$ becomes negative, implying the instability of the HM state towards the separation into the AFM and stable HM phases. However, in the wide region near $n = 1$ (relevant for $SrFeO_3$) the helicoidal state is stable, in agreement with experimental observations.

6. Magnon dispersion

Next we calculate the magnon spectrum for the FM and HM states of the dp model in the leading order of the $1/S$ expansion. Consider small deviations from a perfect helix described

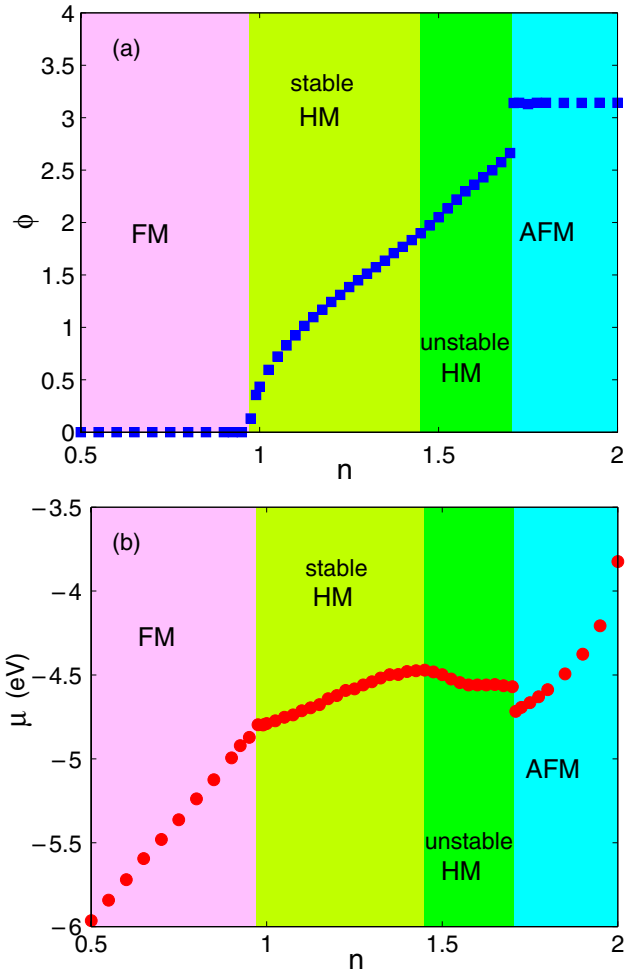

Figure 7. Plotted is the helical angle ϕ (a) and the chemical potential μ (b) versus the hole density n for $(\mathrm{pd}\sigma) = 1.7$ eV, $t_{\mathrm{pp}} = 0.65$ eV and $\Delta = -2$ eV.

by the spherical angles $\theta_j \ll 1$ and ϕ_j in the rotated spin frame:

$$v_j = \mathrm{e}^{\mathrm{i}\frac{\sigma_x}{2}(\mathbf{Q}\mathbf{x}_j)} \begin{pmatrix} -\frac{\theta_j}{2}\mathrm{e}^{-\mathrm{i}\phi_j} \\ 1 - \frac{\theta_j^2}{8} \end{pmatrix}. \tag{25}$$

The quantization of the spin excitations is done using the relation between the spherical angles and the Holstein–Primakoff boson operators [43],

$$\begin{aligned} S_j^+ &\approx S\theta_j \mathrm{e}^{\mathrm{i}\phi_j} = \sqrt{2S}a_j \\ S_j^- &\approx S\theta_j \mathrm{e}^{-\mathrm{i}\phi_j} = \sqrt{2S}a_j^\dagger . \\ S_j^z &= S - a_j^\dagger a_j \end{aligned} \tag{26}$$

The Hamiltonian describing the magnon–hole interaction has the form

$$H_{\mathrm{int}} = -\sqrt{\frac{1}{2S}} \sum_{j\alpha b} t_{\alpha b} \left(d_{j\alpha}^\dagger P_{jb\uparrow} a_j + a_j^\dagger P_{jb\uparrow}{}^\dagger d_{j\alpha} \right) - \frac{1}{4S} \sum_{j\alpha b} t_{\alpha b} a_j^\dagger a_j \left(d_{j\alpha}^\dagger P_{jb\downarrow} + P_{jb\downarrow}{}^\dagger d_{j\alpha} \right), \tag{27}$$

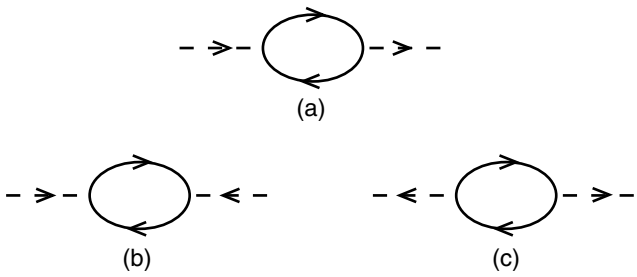

Figure 8. The diagrams contributing to the magnon dispersion in the leading order of the $1/S$ expansion. The solid (dashed) lines are the hole (magnon) propagators.

where we have neglected the terms of higher order in powers of $1/\sqrt{S}$. In the momentum space

$$H_{\rm int} = -\sqrt{\frac{1}{2SN}} \sum_{\mathbf{k}\alpha b} t_{\alpha b} \left(d^{\dagger}_{\mathbf{k+q}\alpha} P_{\mathbf{k}b\uparrow} a_{\mathbf{q}} + a^{\dagger}_{\mathbf{q}} P_{\mathbf{k}b\uparrow}{}^{\dagger} d_{\mathbf{k+q}\alpha} \right) - \frac{\langle T_{\rm dp} \rangle}{4S} \sum_{\mathbf{q}} a^{\dagger}_{\mathbf{q}} a_{\mathbf{q}} \tag{28}$$

where

$$T_{\rm dp} = \frac{1}{N} \sum_{\mathbf{k}\alpha b} t_{\alpha b} \left(d^{\dagger}_{\mathbf{k}\alpha} P_{\mathbf{k}b\downarrow} + P_{\mathbf{k}b\downarrow}{}^{\dagger} d_{\mathbf{k}\alpha} \right)$$

is the kinetic energy of the dp hopping per octahedron. Since the second term in equation (28) already contains the factor $1/S$, the kinetic energy operator can be replaced by its average.

The magnon action is obtained by integrating out holes, which amounts to calculating the loop diagrams shown in figure 8, where solid (dashed) lines are the hole (magnon) propagators. In the FM state spin projection is conserved and only the diagram figure 8(a) is nonzero. The ferromagnon spectrum for $(\mathrm{pd}\sigma) = 1.8$ eV, $t_{\rm pp} = 0.6$ eV and $\Delta = -2$ eV is shown in figure 9. For small wavevectors q the spectrum is anomalously soft due to proximity to the quantum critical point, at which the spin ordering becomes helicoidal. At the critical point the spin stiffness vanishes and the transition temperature drops to zero due to large spin fluctuations. However, such a quantum critical behaviour can be masked by anisotropic spin interactions inevitably present in realistic materials, which open a gap in the magnon spectrum and suppress spin fluctuations. This may explain why no decrease of magnetic transition temperature was observed [41, 42].

In figure 10 we show the magnon spectrum for the helicoidal state with $\mathbf{Q} = 0.93(1, 0, 0)$, which is the ground state for $(\mathrm{pd}\sigma) = 1.7$ eV, $t_{\rm pp} = 0.65$ eV and $\Delta = -2$ eV. In the HM state all three diagrams in figure 8 are nonzero and the magnon dispersion is linear both close to $\mathbf{q} = 0$ and close to $\mathbf{q} = \mathbf{Q}$ (see the inset in figure 10). Note also that for $0 < q < Q$ the magnon spectrum is extremely soft.

Finally, we note that for large negative Δ the HM state is energetically more favourable than canted AFM states. That can be checked numerically, but it is also clear from the fact that the softening of the ferromagnon spectrum occurs at $Q = 0$ (the spin stiffness vanishes) rather than at a finite Q, which would be the case for the transition to a canted AFM state. The absence of the finite-Q instability is related to the fact that the Fermi surface of a strongly covalent dp metal is, in general, not nested.

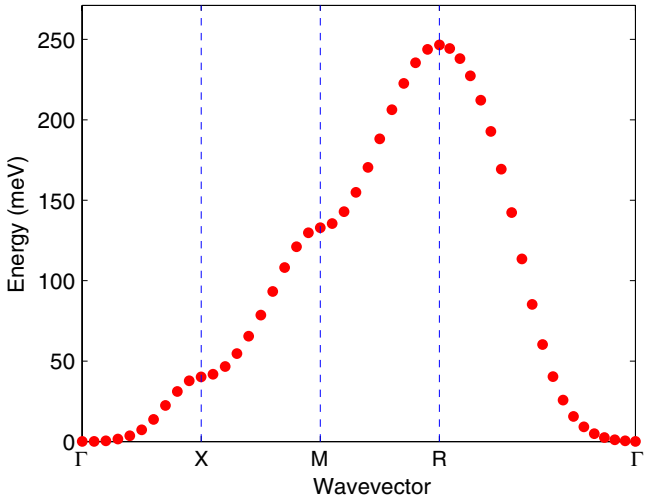

Figure 9. The magnon spectrum for the ferromagnetic state, which is the ground state for $(\mathrm{pd}\sigma) = 1.8$ eV, $t_{\mathrm{pp}} = 0.65$ eV and $\Delta = -2$ eV.

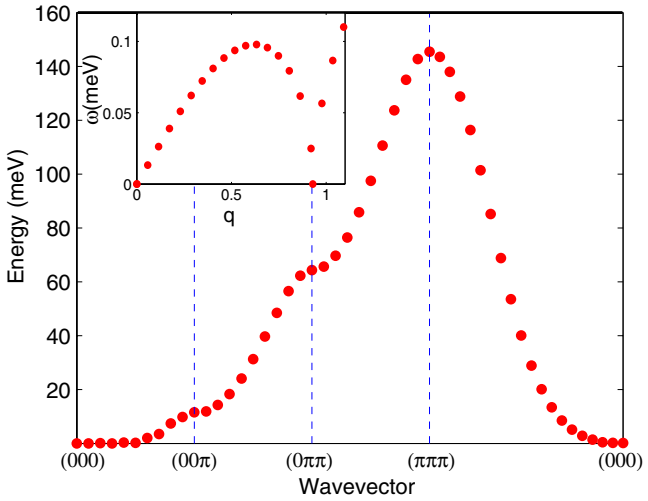

Figure 10. The magnon spectrum for the helicoidal state with $\mathbf{Q} = 0.93(0, 0, 1)$, which is the ground state for $(\mathrm{pd}\sigma) = 1.7$ eV, $t_{\mathrm{pp}} = 0.65$ eV and $\Delta = -2$ eV. The inset shows $\omega_{\mathbf{q}}$ for $\mathbf{q} = q(100)$, where q varies between 0 and $\sim 1.2Q$.

7. Conclusions

We have shown that the antiferromagnetic superexchange between local spins may not be the main reason for non-collinear magnetic ordering in double exchange systems. The double exchange alone can favour helicoidal ordering. Although the transition from ferromagnetic to helicoidal state narrows conduction bands, the energy of the Fermi sea is lowered due to the mixing of the spin-up and spin-down bands.

The ferromagnetic state in transition metal oxides can become unstable even for infinitely strong Hund's rule coupling on transition metal sites, provided that the charge carriers occupy

with a high probability oxygen sites. We have argued that the helicoidal ordering observed in iron perovskites $SrFeO_3$ and $CaFeO_3$ with negative charge transfer energy Δ results largely from the double exchange. We considered a simple double exchange model of dp metals with strongly hybridized transition metal and oxygen orbitals. Using the parameters deduced for $SrFeO_3$ from photoemission experiments, we obtained the helicoidal magnetic ground state.

This approach gives us a consistent picture of structural and magnetic properties of ferrates and explains the difference between the isovalent ferrates and manganites. On the one hand, the large negative Δ suppresses orbital ordering by making these materials more metallic than manganites and by removing the Fermi surface nesting. On the other hand, it favours the helicoidal magnetic ordering, which does not occur in manganites. Furthermore, the helicoidal state favoured by the double exchange is stable with respect to phase separation, in contrast to the instability of the de Gennes canted state, resulting from the competition between the double exchange and superexchange. This explains why the magnetic phase separation, which is widely observed in manganites, does not seem to play an important role in ferrates.

Acknowledgments

It is a pleasure to thank A Boris, B Keimer, G Khaliullin, D Khomskii, G Rozenberg, O Sushkov, B Simons and C Ulrich for many interesting discussions.

Appendix

To clarify the origin of the helicoidal magnetism in double exchange systems, consider a simple continuous model

$$H = \int \mathrm{d}^D x\, \psi^\dagger \left[-\triangle - I\,(\boldsymbol{\sigma}\mathbf{m})\right] \psi, \tag{A.1}$$

describing conducting electrons in the non-degenerate band

$$\psi(\mathbf{x}) = \begin{bmatrix} \psi_\uparrow(\mathbf{x}) \\ \psi_\downarrow(\mathbf{x}) \end{bmatrix}$$

interacting with classical spins of unit length $\mathbf{m}(\mathbf{x})$. In equation (14) I is the Hund's rule coupling and D is the dimension of the space.

We assume that in the ground state spins are confined to the xz plane,

$$\mathbf{m}(\mathbf{x}) = \hat{z}\cos\theta(\mathbf{x}) + \hat{x}\sin\theta(\mathbf{x}), \tag{A.2}$$

in which case the Hamiltonian (A.1) is real and

$$\boldsymbol{\sigma}\cdot\mathbf{m} = \mathrm{e}^{-\mathrm{i}\frac{\sigma_y}{2}\theta}\sigma_z\mathrm{e}^{+\mathrm{i}\frac{\sigma_y}{2}\theta}. \tag{A.3}$$

The spin rotation

$$\psi(\mathbf{x}) = \mathrm{e}^{-\mathrm{i}\frac{\sigma_y}{2}\theta(\mathbf{x})}\psi'(\mathbf{x}). \tag{A.4}$$

aligns the z axis parallel to $\mathbf{m}(\mathbf{x})$. In this spin frame the Hamiltonian has the form

$$H = \int \mathrm{d}^D x\, \psi'^\dagger \left[\left(\hat{\mathbf{p}} - \mathbf{A}\frac{\sigma_y}{2}\right)^2 - I\sigma_z\right] \psi', \tag{A.5}$$

where $\hat{\mathbf{p}} = -\mathrm{i}\nabla$ is the momentum operator and $\mathbf{A} = \nabla\theta$ is the vector potential generated by the rotation in the spin space.

For the helicoidal magnetic state with the wavevector $\mathbf{Q}$, $\theta(\mathbf{x}) = \mathbf{Q}\cdot\mathbf{x}$ and $\mathbf{A} = \mathbf{Q}$. Without loss of generality we can assume that $\mathbf{Q} = Q\hat{z}$. The single-particle Hamiltonian in the momentum space is

$$\hat{h} = k^2 + \frac{Q^2}{4} - (I\sigma_z + Qk_z\sigma_x)\,. \tag{A.6}$$

The electron spectrum for the helicoidal state consists of two bands with the dispersion

$$\varepsilon_{\mathbf{k}}^{(\pm)} = k^2 + \frac{Q^2}{4} \pm \sqrt{Q^2k_z^2 + I^2}. \tag{A.7}$$

The upward shift of the bottom of the conduction band $+\frac{Q^2}{4}$ in the continuous model corresponds to the band narrowing in lattice double exchange models, when the ferromagnetic spin ordering ($Q = 0$) changes to a helicoidal one. The third term in equation (A.7) describes the band splitting due to the mixing of the spin-up and spin-down states in the helicoidal state. This splitting decreases the energy of the occupied states in the lower band, which drives the transition to the helicoidal state.

The optimal helix wavevector Q is found from

$$\frac{\mathrm{d}}{\mathrm{d}Q}\,(\varepsilon - \mu n) = 0, \tag{A.8}$$

where

$$n = \int \frac{\mathrm{d}^D k}{(2\pi)^D}\,\theta(\mu - \varepsilon_{\mathbf{k}}^{(-)}), \tag{A.9}$$

$$\varepsilon = \int \frac{\mathrm{d}^D k}{(2\pi)^D}\,\theta(\mu - \varepsilon_{\mathbf{k}}^{(-)})\varepsilon_{\mathbf{k}}^{(-)}, \tag{A.10}$$

are respectively the density and energy density of electrons and we have assumed that only the lower electron band is occupied. Here energy is minimized at constant density n and the chemical potential μ plays the role of the Lagrange multiplier. The minimization of energy at constant μ gives rise to a strong dependence of the electron density n on the helix wavevector Q. In reality, large deviations of the average electron density are suppressed by Coulomb interactions, not included in the free electron model (A.1).

The ferromagnetic state becomes unstable when

$$\left.\frac{\mathrm{d}}{\mathrm{d}Q^2}\,(\varepsilon - \mu n)\right|_{Q=0} = \frac{1}{4}\int_{k<k_\mathrm{F}} \frac{\mathrm{d}^D k}{(2\pi)^D}\left(1 - \frac{2k_z^2}{I}\right) = \frac{n}{4}\left(1 - \frac{2k_\mathrm{F}^2}{(D+2)I}\right) = 0, \tag{A.11}$$

where k_F is the Fermi momentum. Since the electron dispersion for the ferromagnetic state is $\varepsilon_{\mathbf{k}}^{(\pm)} = k^2 \pm I$, the critical value of the critical potential is given by

$$\mu_\mathrm{c} = k_\mathrm{F}^2 - I = \begin{cases} \dfrac{I}{2}, & \text{for } D = 1, \\ I, & \text{for } D = 2, \\ \dfrac{3I}{2}, & \text{for } D = 3. \end{cases} \tag{A.12}$$

In one dimension, the instability occurs when the chemical potential is smaller than the lowest energy of the unoccupied (spin-down) band, $\mu_\mathrm{c} < I$, while in two dimensions the chemical potential touches the bottom of the unoccupied band at the critical point. For $D = 3$, the assumption that only the lower band is occupied is not valid. In this case the transition to the helicoidal state does not occur, as the unsaturated ferromagnetic state with partially occupied spin-up and spin-down bands has lower energy. The absence of transition is related to a low density of spin-flip excitations in three dimensions.

References

[1] Korotin M A, Anisimov V I, Khomskii D I and Sawatzky G A 1998 *Phys. Rev. Lett.* **80** 4305
[2] Anisimov V I, Korotin M A, Zölfl M, Pruschke T, Le Hur K and Rice T M 1999 *Phys. Rev. Lett.* **83** 364
[3] Zener C 1951 *Phys. Rev.* **81** 440
Zener C 1951 *Phys. Rev.* **82** 403
[4] Anderson P W and Hasegawa H 1955 *Phys. Rev.* **100** 675
[5] de Gennes P-G 1960 *Phys. Rev.* **118** 141
[6] Kubo K and Ohata N 1972 *J. Phys. Soc. Japan* **33** 21
[7] See e.g., Tokura Y (ed) 2000 *Colossal Magnetoresistive Manganites* (New York: Gordon and Breach)
[8] Takeda T, Yamaguchi Y and Watanabe H 1972 *J. Phys. Soc. Japan* **33** 967
[9] Oda H, Yamaguchi Y, Takei H and Watanabe H 1977 *J. Phys. Soc. Japan* **42** 101
[10] Kawasaki S, Takano M, Kanno R, Takeda T and Fujimori A 1998 *J. Phys. Soc. Japan* **67** 1529
[11] Woodward P M, Cox D E, Moshopoulou E, Sleight A W and Morimoto S 2000 *Phys. Rev.* B **62** 844
[12] See Geck J, Büchner B, Hücker M, Klingeler R, Gross R, Pinsard-Gaudart L and Revcolevschi A 2001 *Phys. Rev.* B **64** 144430 and references therein
[13] Kawano-Furukawa H, Kajimoto R, Yoshizawa H, Tomioka Y, Kuwahara H and Tokura Y 2003 *Phys. Rev.* B **67** 174422
[14] For a review see e.g., Dagotto E, Hotta T and Moreo A 2001 *Phys. Rep.* **344** 1
[15] Inoue J and Maekawa S 1995 *Phys. Rev. Lett.* **74** 3407
[16] Li M-Z, Zou L-J and Zheng Q Q 1998 *J. Phys.: Condens. Matter* **10** L521
[17] Nagaev E L 1974 *Phys. Status Solidi* b **65** 11
[18] Arovas D P and Guinea F 1998 *Phys. Rev.* B **58** 9150
[19] Kagan M Yu, Khomskii D I and Mostovoy M V 1999 *Eur. Phys. J.* B **12** 217
[20] Soloviev I V and Terakura K 2001 *Phys. Rev.* **63** 174425
[21] Jensen J and Makintosh A K 1991 *Rare Earth Magnetism* (Oxford: Oxford University Press)
[22] Kasuya T 1996 *Magnetism* vol IIB, ed G T Rado and H Suhl (New York: Academic) p 215
[23] Wang X 1998 *Phys. Rev.* B **57** 7427
[24] Vogt M, Santos C and Nolting W 2001 *Phys. Status Solidi* b **223** 679
[25] Mostovoy M 2004 *Preprint* cond-mat/0409068
[26] Millis A J, Littlewood P B and Schraimann B I 1995 *Phys. Rev. Lett.* **74** 5144
[27] MacChesney J B, Sherwood R C and Potter J F 1965 *J. Chem. Phys.* **43** 1907
[28] Adachi H and Takano M 1991 *J. Solid State Chem.* **93** 556
[29] Takano M, Nasu S, Abe T, Yamamoto K, Endo S, Takeda Y and Goodenough J B 1997 *Phys. Rev. Lett.* **67** 3267
[30] Gallagher P K, MacChesney J B and Buchanan D N E 1966 *J. Chem. Phys.* **45** 2466
[31] Dann S E, Weller M T, Currie D B, Thomas M F and Al-Rawwas A D 1993 *J. Mater. Chem.* **3** 1231
[32] Kuzushita K, Moritomo A, Nasu S and Nakamura S 2000 *J. Phys. Soc. Japan* **69** 2767
[33] Lebon A, Adler P, Bernhard C, Boris A V, Pimenov A V, Maljuk A, Lin C T, Ulrich C and Keimer B 2004 *Phys. Rev. Lett.* **92** 037202
[34] Bocquet A E, Mizokawa T, Saitoh T, Namatame H and Fujimori A 1992 *Phys. Rev.* B **46** 3771
[35] Matsuno J, Mizokawa T, Fujimori A, Takeda Y, Kawasaki S and Takano M 2002 *Phys. Rev.* B **66** 193103
[36] Goodenough J B and Zhou J-S 1998 *Chem. Mater.* **10** 2980
[37] Alonso J A, García-Muñoz J L, Fernández-Díaz M T, Aranda M A G, Martínez-Lope M J and Casais M T 1999 *Phys. Rev. Lett.* **82** 3871
[38] Mizokawa T, Khomskii D I and Sawatzky G A 2000 *Phys. Rev.* B **61** 11263
[39] Slater J C and Koster G F 1954 *Phys. Rev.* **94** 1498
[40] Mahadevan P, Shanthi N and Sarma D D 1996 *Phys. Rev.* B **54** 11199
[41] Nasu S 2000 *Hyperfine Interact.* **128** 101
[42] Nasu S, Kawakami T, Kawasaki S and Takano M 2002 *Hyperfine Interact.* **144/145** 119
[43] Furukawa N and Motome Y 2003 *Physica* B **329** 759